Journal Pre-proofs

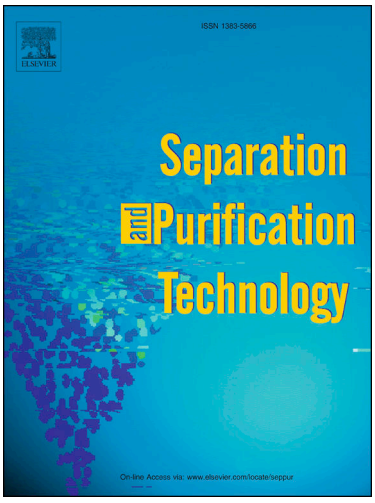

Membranes Based on Polyacrylamide Coatings on Metallic Meshes Prepared by a Two-Steps Redox Polymerization. Performance for Oil-Water Separation and Biofouling Effects

J. Nicolás Cabrera, Graciela Rojas, Norma B. D'Accorso, Leonardo Lizarraga, R. Martín Negri

PII: S1383-5866(20)31440-4
DOI: https://doi.org/10.1016/j.seppur.2020.116966
Reference: SEPPUR 116966

To appear in: *Separation and Purification Technology*

Received Date: 21 November 2019
Revised Date: 16 March 2020
Accepted Date: 16 March 2020

Please cite this article as: J. Nicolás Cabrera, G. Rojas, N.B. D'Accorso, L. Lizarraga, R. Martín Negri, Membranes Based on Polyacrylamide Coatings on Metallic Meshes Prepared by a Two-Steps Redox Polymerization. Performance for Oil-Water Separation and Biofouling Effects, *Separation and Purification Technology* (2020), doi: https://doi.org/10.1016/j.seppur.2020.116966

This is a PDF file of an article that has undergone enhancements after acceptance, such as the addition of a cover page and metadata, and formatting for readability, but it is not yet the definitive version of record. This version will undergo additional copyediting, typesetting and review before it is published in its final form, but we are providing this version to give early visibility of the article. Please note that, during the production process, errors may be discovered which could affect the content, and all legal disclaimers that apply to the journal pertain.

© 2020 Published by Elsevier B.V.

Journal Pre-proofs

Membranes Based on Polyacrylamide Coatings on Metallic Meshes Prepared by a Two-Steps Redox Polymerization. Performance for Oil-Water Separation and Biofouling Effects

J. Nicolás Cabrera[1,2,3], Graciela Rojas[4], Norma B. D'Accorso[5,6], Leonardo Lizarraga[3], R. Martín Negri[1,2*] .

1. Departamento de Química Inorgánica, Analítica y Química Física. Facultad de Ciencias Exactas y Naturales. Universidad de Buenos Aires. Argentina.
2. Instituto de Química Física de Materiales, Medio Ambiente y Energía (INQUIMAE). Consejo Nacional de Investigaciones Científicas y Técnicas (CONICET)-Universidad de Buenos Aires.
3. Centro de Investigación en Bionanociencias (CIBION). CONICET.
4. YPF Tecnología (Y-TEC). Argentina.
5. Departamento de Química Orgánica. Facultad de Ciencias Exactas y Naturales. Universidad de Buenos Aires.
6. Centro de Investigaciones en Hidratos de Carbono (CIHIDECAR). CONICET-Universidad de Buenos Aires.

*** Corresponding autor: R. Martín Negri: rmn@qi.fcen.uba.ar.**
Address: Ciudad Universitaria, Pabellón II. C1428EGA, Buenos Aires, Argentina.

Abstract

Superhydrophilic oil-water separation membranes were prepared based on chemical (non-photo-induced) polymerization of acrylamide on metal meshes. Membranes were characterized by surface morphological analysis (SEM and AFM), determination of contact angles of water and oil drops, measurement of water flow through the membranes, analysis of dissolved organic in filtered water-oil systems, critical intrusion pressure of oil and surface coverage by bacterial biofilms. The main characteristics of the membranes were studied as function of coverage with polyacrylamide (PAM). The membranes presented efficiencies larger than 99% for toluene-water separation and lifetimes of several months. The intrusion pressure (0.25-1.25 kPa) and water flow (10-300 $Lm^{-2}s^{-1}$) varied depending on PAM coverage. A mathematical model was implemented for predicting the water flow as function of hydrogel coverage.

The results indicate there is a degree of compromise between three factors that are related to the amount of PAM coating: avoiding biofouling (which can block the flow, induce corrosion, etc.), maintaining an important flow of water and sustaining a given intrusion pressure of oil on the membranes.

***Keywords*:** Polyacrylamide, Superhydrophilic Membranes, Oil-Water Separation, Biofilms.

1. Introduction

In recent decades there has been a growing interest in developing new superhydrophilic and superhydrophobic membranes **[1, 2]**. The driving force to improve this technology is the petroleum industry, which uses huge amounts of water to extract the hydrocarbons. The water-oil mixture, generally with much higher percentages of water than hydrocarbon, is usually separated by gravitational decantation, but given the slowness of this process, it is of high relevance to develop new separation methods, mainly based on membranes that allow one phase to pass while retaining the other. These membranes are classified as superhydrophobic (retaining the aqueous phase) and superhydrophilic (allowing the aqueous phase to pass through). It is possible in principle to use both types of membranes in different sectors of separation reactors.

A superhydrophilic membrane is defined by having water-surface contact angles in air lower than 5°. Additionally, it is desirable for the membrane to be superoleophobic also, given by two characteristics: i) sliding angle oil/surface less than 5°; ii) oil-surface contact angle underwater greater than 150°. Many superhydrophobic surfaces are obtained by electrospinning, for example, by dip-coating electrospun polyimide in decanoic acid and silica nanoparticles **[3]**, a PDMS and ZnO decorated on a self-standing polyimide **[4]**, the combination of electrospun polyimide nanofibers and an in-situ polymerized polybenzoxazine containing silica nanoparticles **[5]** and with a Fe^{3+}–phytic acid/octadecyltrimethoxysilane/polyimide nanofibrous membrane **[6]**.

In a previous article **[7]**, we report the characteristics of superhydrophobic membranes based on electrochemical deposition of stearic acid and the consequent formation of nanotubes of metallic stearate on brass meshes. As a following step, we developed a superhydrophilic membrane, which complements our project. The study and preparation of superhydrophilic membranes for oil-water separation has been receiving wide interest in recent years, including coatings of PVDF meshes **[8]**, polyamides meshes **[9]**, hybrid inorganic-organic coatings **[10,11]** and inorganic coatings **[12, 13, 14, 15, 16]**. As substrates for the membranes, metallic meshes are commonly in petroleum industry because they guarantee the passage of the phase to be filtered (aqueous in this case) through its pores.

In this work superhydrophilic membranes based on polyacrylamide (PAM) coatings on brass metal mesh substrates are presented. As a hydrogel, polyacrylamide consists of a 3D crosslinked polymer

network with water filling interstitial spaces. The natural fluidity of the trapped water confers a liquid like property to gel surfaces and these liquid water-like characteristics determine the highly hydrophilic (in air) and oleophobic (under water) properties of the gel surface **[17, 18]**.

Superhydrophilic PAM membranes have been reported in the scientific literature, but its application at industrial level is limited by the type of photochemical initiation commonly used **[19, 20, 21, 22]**. In fact, the quantity of PAM formed by photopolymerization is limited by the amount of photons from the UV source. In addition, and for the same reason, the polymerization is usually incomplete leaving highly toxic acrylamide (monomer) residue. PAM has been used as additive in filtration-separation membranes **[23, 3, 24, 25]** and as an organic coagulant aid for ultrafiltration **[26, 27, 28, 29]**.

The first objective of this work is to notify the preparation of superhydrophilic membranes based on PAM coated brass meshes, where polymerization is achieved by redox initiation, not photochemical. The second objective is the characterization and modeling of properties related to water filtration and oil phase retention in the membranes. The third objective is to analyze biofilms development on the membranes. It is common that many research works are focused on describing engineering properties using water or saline solutions, but with low bacteria content. However, the formation of biofilms on the superhydrophilic membranes is a crucial point since they usually seal them or produce microbiologically influenced corrosion **[30]**.

2. Materials and Methods

2.1. Chemicals.

All solvents and reagents were of analytical quality and used as received. Acrylamide (AM), *N N′*-methylenebis(acrylamide) (BIS) and polyacrilamide (PAM; average Mr =150000) were purchased from Sigma Aldrich. Ammonium persulfate (APS) and sodium hydroxide (NaOH) were purchased from Anedra (Argentina). Petroleum samples from an Argentinean oil field were provided by YPF-Tecnología SA (Y-TEC): *light crude* (density ≈ 0.75 g/cm^3, viscosity ≈ 0.9 cP, at 25 °C) and , *heavy crude* (density ≈ 0.92 g/cm^3). Sunflower oil was purchased from a local store (density ≈ 0.91 g/cm^3). Brass meshes (porous diameter ≈ 77 μm, atomic ratio Cu/Zn=4) were provided by Sueiro & Hijos (Argentina). These meshes are typically used in several oil-water and waste-water separation processes at industrial level.

2.2 Preparation of polyacrylamide (PAM) coated meshes.

Brass meshes were washed with acetone, de-ionized water and diluted acid solution prior its use. Then, meshes were pre-treated with ammonium persulfate (APS) as detailed in **[31]** by immersing in a 0.05 M APS and 1 M NaOH solution for 30 minutes. Afterwards, meshes were rinsed with abundant de-ionized water and dried in oven at 70 ºC at atmospheric pressure. Dark blue colored meshes were obtained by this procedure, referred as the pre-treated meshes from now on.

Then, the pre-treated meshes were immersed in a mixture of AM (monomer), BIS (linker), and APS (initiator) in water at room temperature (≈ 25 °C). A small amount of PAM was added in order to increase viscosity and, hence, the adherence of organic material to the mesh. AM concentration was 0.75 M and the weight proportion was 1- 0.03- 0.02- 0.01 for AM- BIS- APS- PAM. The immersion time was about 3 seconds. After immersion, the meshes were dried at 70 ºC and atmospheric pressure for 10 minutes. Then, the meshes were re-immersed for a given amount of cycles: 1, 3, 5 and 7 cycles were tested. The number of immersion cycles in the PAM solution is referred as **N**. Meshes were dried after each immersion cycle, as indicated. Afterwards, samples were placed in an oven at 70 ºC during 6 hours for polymerizing. After polymerization, PAM membranes were hydrated in de-ionized water for 24 hours, remaining underwater for further tests.

Additionally, polyacrylamide was synthesized in a separate flask (under identical conditions than for membranes) in order to characterize the polymer apart from the metallic mesh.

2.3 Instrumentation.

Surface morphology was analyzed using a Field Emission Scanning Electron Microscope (FESEM; Zeiss Supra 40 Gemini). Infrared spectra (ATR and transmission) were recorded using Nicolet 8700 equipment. Ultra violet absorption spectrums were determined using a Shimadzu UV-3101PC spectrometer.

Liquid ^{1}H NMR spectrum was recorded on a Bruker AC-200 spectrometer operating at 200 MHz on the swollen polymer. High-resolution ^{13}C NMR solid-state spectrum was recorded using a CP-MAS pulse sequence (cross polarization and magic angle spinning) with proton decoupling during acquisition, at room temperature, in a 7T Bruker Avance II-300 spectrometer equipped with a 4-mm MAS probe. The operating frequency was 75.46 MHz. Glycine was used as an external reference for the ^{13}C NMR spectrum and to set the Hartmann-Hahn matching condition in the cross-polarization

experiments. The recycling time was 6 s. Contact time during CP was 2 ms. The spinning rate was 10 kHz.

Differential Scanning Calorimetry (DSC) measurements were performed using a TA Q20 differential scanning calorimeter in a dry nitrogen atmosphere. Indium standard was used for calibration. Mass of 5-10 mg of each sample were placed in the DSC pan. Samples were first heated to 200 °C and held at temperature for 10 min to remove the thermal history. Then, samples were cooled to -20°C at a rate of 10 °C/min, held for 10 min, and again heated to 210 °C at 10 °C/min. The glass transition values (Tg) were taken as the midpoint of the transition in the second heating scan.

Thermogravimetric analysis (TGA) of the sample samples were performed using a Shimadzu TGA-51 under nitrogen atmosphere, with a heating rate of 10 °C/min and a gas flux of 30 mL/min.

Atomic force microscopy (AFM) images were acquired using a Bruker Multimode 8 SPM (Santa Barbara, CA, USA) and NanoScope V Controller (Santa Barbara, CA, USA). The image analysis was performed using Gwyddion version 2.46 (Brno, Czech Republic) and Nanoscope version 9.1 software (Santa Barbara,CA, USA). The AFM images were acquired in the intermittent mode using silicon tips doped with antimony, with a spring constant of 42 N/m and a resonance frequency of 320 kHz. Areas of typically 10 μm × 10 μm were scanned. Average surface roughness was determined from AFM height images **[32]**. For each height image, a reference plane (mean plane) was defined, and a Z-axis perpendicular to that plane was considered, with Z = 0 on the plane. Z-values were calculated from the images in a discrete manner, where Zj was defined as the height of the jth-pixel from the mean plane. That is, Z is a discrete stochastic variable. Positive Z-values are associated to protrusions above the mean plane, while negative Z-values, to depressions below the plane. The average surface roughness (**R_a**) of each AFM image was determined as the average deviation of height values from the mean plane, when considering M pixels in a given image: $R_a = \frac{1}{M}\sum_{j=1}^{M}\left|Z_j\right|$ (M = 262,144).

2.4 Swelling ratio.

The swelling ratio of the polymer was determined following the protocol detailed in **[33]** with some modifications. Briefly, a weighed amount of the polymer was immersed in 300 mL of de-ionized water at 25 ºC shaking at 100 rpm. The polymer was separated from the de-ionized water at defined time intervals, carefully wiped with paper, and then weighed. Swelling ratio (*M*) was calculated as $M = \frac{w_2 - w_1}{w_1}$, where w_2 is the weight of the swollen polymer and w_1 the initial weight of the polymer.

2.5 Water-air and chloroform-underwater contact angles.

Water in air contact angles (**WA-CA**) were determined using a homemade device that was calibrated with a KSV CAM 200 Optical Contact Angle Meter. Images were analyzed with an appropriate Image J software plugin. Contact angles were determined by analyzing 3 drops on each membrane and on three different replicated membranes. Thus, for each type of prepared membrane a total of 9 values were obtained, which were averaged. All determinations were performed at room temperature (≈ 25 °C) and atmospheric pressure. The volume of the water droplet was 50 μL and **WA-CA** angles were registered after 1 minute since drop deposition on the surface.

The oil underwater contact angles (**OW-CA**) were measured in different set-ups, depending if the oil was lighter or heavier than water. In the case of light-crude (0.75 g/cm^3) and sunflower oil (0.95 g/cm^3) the membranes were placed on a membrane holder at the top of an acrylic fishbowl designed for this purpose. The acrylic box was filled with water, while oil was bubbled from the bottom using *ad hoc* holes where glass pipettes containing the oil were introduce. Thus, oil drops goes up in the water until getting into contact with the membranes, where an image is recorded for **OW-CA** determination.

On the other hand, chloroform was used as organic heavier than water (1.4 g/cm^3). In that case, chloroform drops were slowly placed on the membrane surface underwater for **OW-CA** determinations.

2.6 Water flux measurement.

Membranes were placed in another *ad hoc* designed glass container for water flow studies. This container is composed of two identical glass tubes of 17.5 cm length and 2.5 cm diameter, each one having an appropriated seat-beading at one extreme for placing the membranes, which separates both tubes. Thus, the *tube-membrane-tube* system can be placed vertically or horizontally, depending on the application. Water flux through the membrane was determined by measuring the volume of vertically collected water through the membrane during a fixed time (typically 40-50 seconds) while maintaining a constant water column of 5 cm on the membrane.

2.7 Critical intrusion pressure (**P_c**).

The critical oil intrusion pressure, **P_c**, is defined as the maximum pressure exerted by the column height of given oil that the membrane can supports without permeating any drop of oil. The membranes were vertically placed in the system *tube-membrane-tube* for **P_c** determinations, adding oil on the top of the membrane. The critical intrusion height of the for sunflower oil was determined for three replicates of each membrane. The values of **P_c** were calculated by experimentally determining the

maximum height of oil that is supported by the membrane ($\mathbf{H_c}$) by $\mathbf{P_c} = \delta_{oil}\, g\, \mathbf{H_c}$, were δ_{oil} is the density of the specific oil used in the test.

2.8 Oil-water separation efficiency.

The oil-water separation efficiency was evaluated by determining the amount of residual toluene in water after separating a toluene-water mixture. Mixtures consisted of 3 mL of toluene and 3 mL of distilled water, vigorously shaked and poured on top of the membrane in the vertical set up *tube-membrane-tube*. Then, the aqueous phase was collected after passing through the membrane. The amount of toluene in the collected phase was determined by chloroform extraction followed by UV spectroscopic determinations of toluene concentration.

2.9 Exposure to harsh conditions

Three cycles membranes were tested to study their stability under four different harsh conditions, saline water (NaCl 1M), hard water ($MgCl_2$ 1M, $CaCl_2$ 1M), acid solution (pH=3, HCl) and alkaline solution (pH=11, NaOH). Membranes were immersed in these solutions during 24 hours and then chloroform underwater contact angle and intrusion pressure were determined.

2.10 Bacterial adhesion assay

Bacterial adhesion assays were performed with the Gram negative bacteria *Pseudomonas protegens*. These were inoculated in LB media (5g/L yeast extract, 10g/L peptone and 5g/L sodium chloride) and incubated overnight at 30 ºC. Overnight *Pseudomonas* cultures were diluted to an optical density of 0.05 (600 nm, 1cm path length) in LB media and incubated again overnight at 30 ºC. The studied membranes were cut into small pieces and sterilized by immersion in ethanol 70% solution during 24 hours. Then, these pieces were set in a 24 multiwell plate, where 1 ml of the growth *Pseudomonas* media was added and incubated at 30 ºC. After a given time (1, 3, 5 or 24 hours), the surfaces were rinsed with de-ionized water and dried over air. All assays were performed three times. This protocol is similar to others previously reported **[34, 35]**.

All the samples were imaged using AFM in intermittent mode **[36]** with the same parameters described previously. The images were analyzed to determine the percentage of the total area covered by bacteria in each of the AFM images. Bacteria detection was performed by thresholding and filtering using Gwyddion software.

3. Results and Discussions

3.1 Characterization.

The first result concerns with the needed of pre-treatment. Meshes coated with PAM, but without the pre-treatment, do not wet homogenously when immersed in the polymerization mix and PAM gathers around on one side of the mesh. Moreover, the mesh-PAM systems obtained without pre-treatment are waterproof without observing water flux through it. Therefore, only membranes with the pre-treatment are considered from now on.

Figures 1 a-b-c show SEM images of a pre-treated mesh without PAM (only first stage, before immersion in the polymerization mixture, **N**=0) showing that pre-treatment with APS induces rod shaped nanostructures.

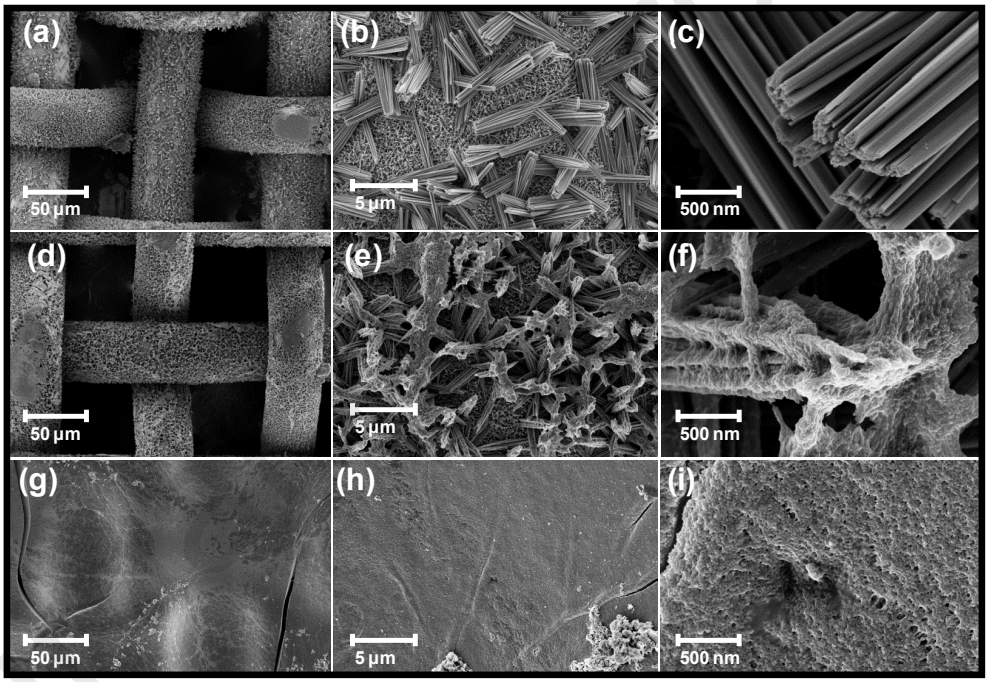

Figure 1. SEM images of PAM membranes prepared with different number of immersion cycles: N=0 (Pre-treatment, Figs. a-b-c), N=3 (d-e-f) and N=7 (g-h-i).

When these meshes are immersed in the polymerization mixture (second stage) the PAM coating is observed, which partially covers the metallic filaments and hence forms the membrane (**Figures 1 d-e-f**). In the case of seven immersion cycles (N=7), the PAM coating extends to the entire mesh, not only on the metallic filaments, but filling large part of the pores (**Figures 1 g-h-i).**

The amount of polymer in each type of membrane was studied by thermogravimetric analysis (TGA). It is observed in **Figure 2** that, in every curve, there are two significant weight losses. The loss around 276 ºC can be attributed to elimination of ammonia. At higher temperatures starts the process of chain polymer decomposition. In the case of **N**=1 the amount of polymer is too low to be detected

with our instrument. In all the other cases, the loss of polymer weight increases with **N**. In the case of **N**=7 the mass loss at 700 °C rises up to 35% of the initial **(Figure 2**).

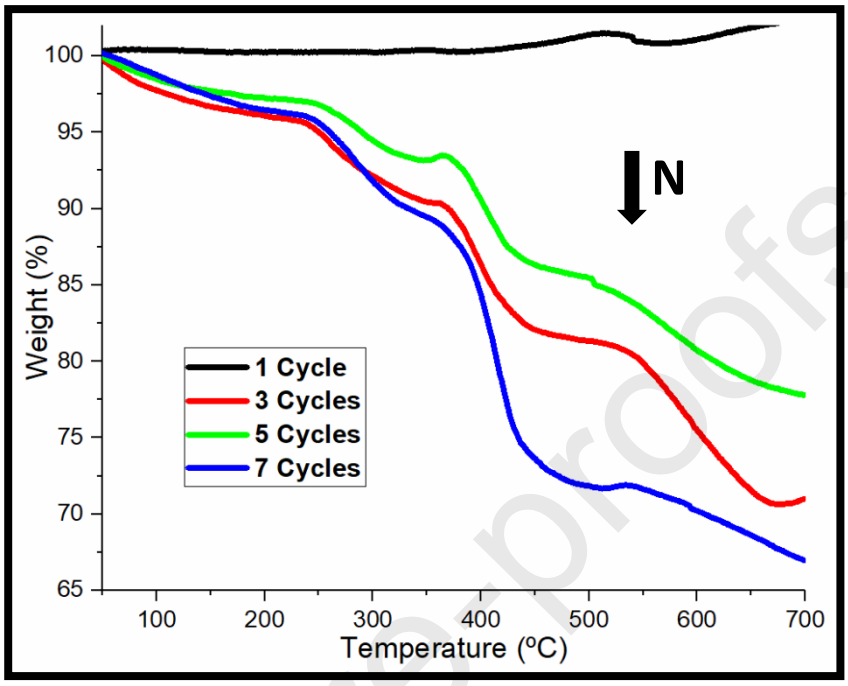

Figure 2. TGA of membranes with different number of immersion cycles (N=1,3,5,7).

Characterizations of the polymer via FTIR, ^{1}H and ^{13}C NMR, and DSC are presented in the supplementary material. **Figure S1** shows the FTIR (ATR) spectrum of membranes, indicating the bands associated to groups expected in PAM and also those assigned to metal–oxygen stretching of CuO and ZnO resulted from oxidation with APS in the first stage (pre-treatment). **Figure S2** shows ^{1}H and ^{13}C NMR spectra, observing the resonance signals of methine and methylene. DSC analysis shows a glass transition temperature at 195 ºC **(Figure S3)**, consistent with reported values **[37]**.

3.2 Hydrophilicity and Oleophobicity.

Examples of the superhydrophilic and superoleofobic behavior are shown in **Figures 3 and 4**, respectively. **Figures 3a-b-c** show how a water drop completely spreads over the surface of the membrane when is deposited from above (water-in-air experiment). Consistently, polymer swelling was observed in all cases when cross-linked PAM was immersed in water. The result of polymer-water swelling experiment is shown in **Figure S4** (Supplementary Material), determining the amount of absorbed water into the polymer as function of time in a water solution. This experiment showed that about eight hours are necessary to get the polymer completely hydrated.

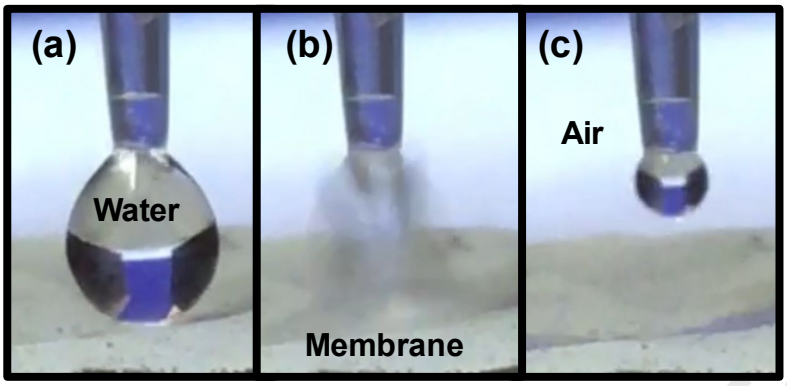

Figure 3. (a) A water drop approaches the membrane from above, using a pipette. (b) When the drop touches the membrane, it begins to spread on the surface. (c) Finally, in a fraction of seconds, the drop is filtered through the membrane and disappears from the surface.

Figure 4a shows a fish tank full of water on whose lid a PAM membrane is placed horizontally. Light oil (0.75 g/cm^3) is bubbled from the bottom. Crude oil bubbles rise through the water up to reaching the membrane surface. On the other hand, in **Figure 4b** the membrane is now placed at the bottom of the fish tank, submerged in water, and a drop of chloroform (1.4 g/cm^3) is injected from the top until it is deposited on the membrane. These experiments allow the so-called " *underwater contact angles of oil* " **(OW-CA)** to be determined for oils lighters and heavier than water.

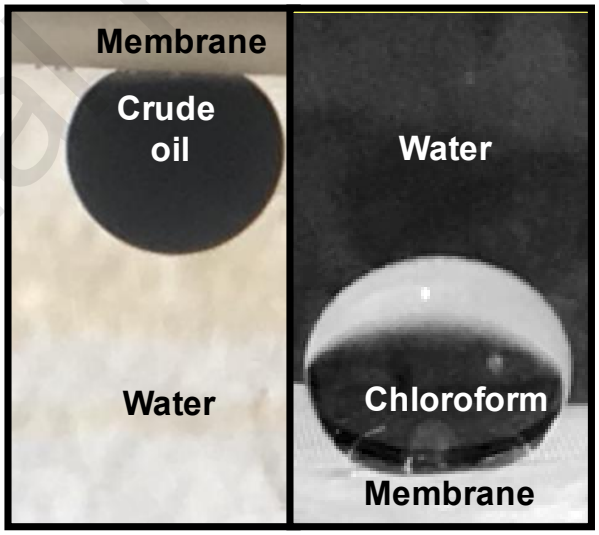

Figure 4. Underwater superoleophobic behavior of prepared membranes. (a) Light Oil (0.75 g/cm^3). (b) Chloroform (1.4 g/cm^3).

Table I shows the water in air (**WA-CA**) and the chloroform underwater (**OW-CA**) contact angles of the studied membranes.

Table I: Contact angles of the studied surfaces.

	Immersion Cycles (N)	Water in air contact angle (WA-CA)	Chloroform underwater contact angle (OW-CA)
Pristine Brass Mesh	-	131º ± 5º	113º ± 10º
First stage: APS Pre-Treatement	0	<5º	155º-165º
Second Stage: PAM Coating	1	<5º	155º-165º
	5	<5º	155º-165º
	10	<5º	155º-165º
	15	<5º	155º-165º

The characteristics shown in **Table 1** remain during several months after membrane preparation if membranes are stored under hydration with de-ionized water.

The first observation in Table 1 is that pre-treatment with APS induces superhydrophilicity (**WA-CA** lower than 5º). This is associated to the nanostructures generated by oxidation with the pre-treatment. The superhydrophilicity is conserved after the second stage (coating with PAM). The second observation is the induction of superoleophobic behavior under water (**OW-CA** larger than 150º).

Note that superhydrophilicity and superoleophobicity are induced by the APS pre-treatment. However, pre-treated meshes (first stage only) do not support oil pressure on it. Hence, in order to obtain membranes which separate oil-water mixtures and filter water while retaining oil on its surface, the PAM coating is required (second stage). This is illustrated in **Figure 5**, where the critical intrusion pressure, $\mathbf{P_c}$ (see Section *2.7*) is plotted as function of the number of coating cycles, **N** ($\mathbf{P_c}$=0 for **N**=0 in **Figure 5**).

Figure 5 shows that $\mathbf{P_c}$ linearly increases with **N**. The non-zero values of $\mathbf{P_c}$ may be related to the fact that coating with PAM sustain permanent hydration of the surface and therefore it is necessary to have a minimum oil pressure on it in order to disrupt the hydration layer, allowing the oil to flow. At a microscopic level, the surface hydration is expected to increase with the amount of hydrogel, that is, with **N**, in agreement with the results of **Figure 5**. A more detailed study at microscopic level should include other factors, mainly the dependence of $\mathbf{P_c}$ with the pore size of the membrane, which is out of the scope of the present work.

Journal Pre-proofs

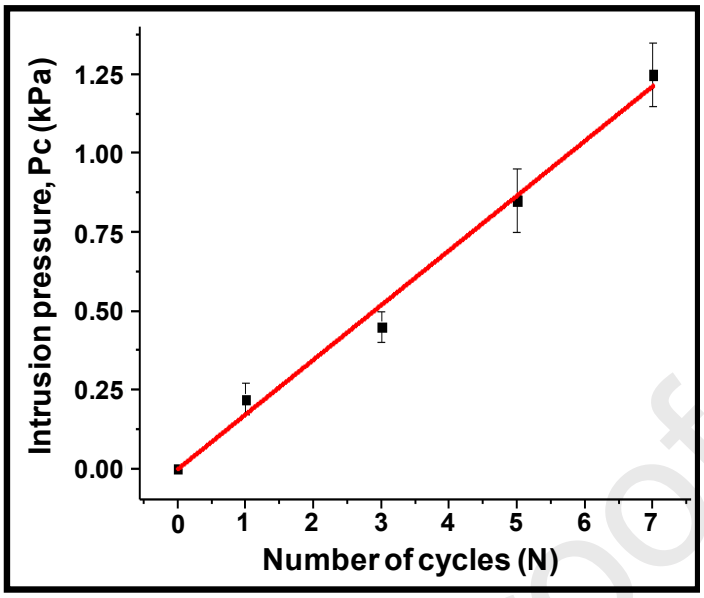

Figure 5. Critical intrusion pressure of sunflower oil vs. the number of immersion cycles.

The coated meshes (**N** ≥ 1) allows to separate oil-water mixtures. An example of the separation quality of the studied membranes is shown in **Figure 6** for the case of a vertical separation, although horizontal separation was successfully achieved as well**.** In **Figure 6** the membrane is placed horizontally, separating two compartments. Initially, **Figure 6a**, a given column height of sunflower oil is supported on the membrane. In **Figure 6b** water droplets (blue colored for contrast) are injected into the upper compartment. In **Figure 6c** an increase of water content is observed in the vessel placed below, indicating that the injected water was completely filtered through the membrane. Water was completely filtrated in few seconds.

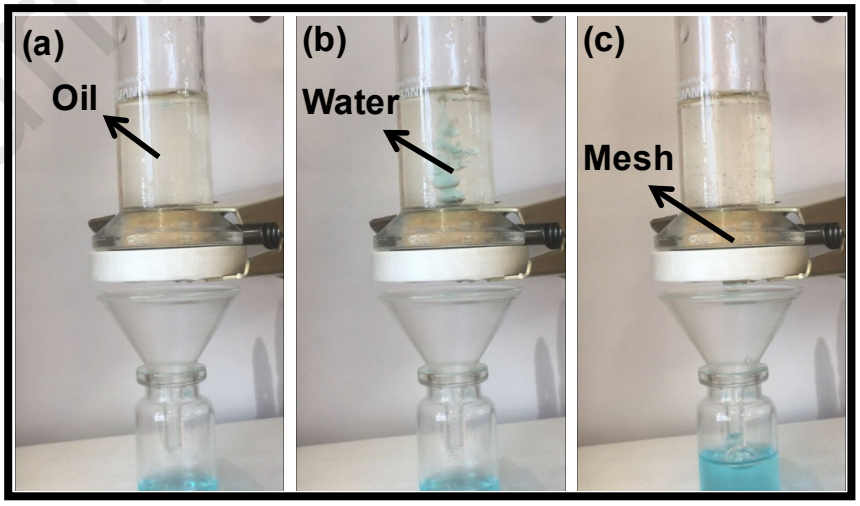

Figure 6. Separation performance of PAM membranes.

The separation described in **Figure 6** was observed for the cases of organic compounds (chloroform, toluene), sunflower oil, light crude and heavy crude. In the experiments of oil/water separation it was not observed significant variation of the water flow with the chemical nature of the oil. The only phase that goes through the membrane is the aqueous phase, carrying only traces of dissolved organics. The variation of the aqueous flow between replicated tests is greater than the variation introduced by changing the organic liquid mixed with water in the upper compartment of the separation tubes. Oil-water separation tests were performed not only with light-oil, but with a sample of heavy oil from Patagonia also (density = 0.92 g/cm3) that was tested with a PAM-coated membrane (**N**= 3), obtaining successful results: only water flows through the system and membranes were not covered by the heavy-oil in at least 10 vertical tests.

No oil-water interfaces were detected at the output of the filtering system in any of the tests. This suggests that the concentration of oil in the filtered phase should be no larger than its saturation concentration in water. **Figure 7** shows the residual amount of toluene in water after the separation assays of toluene and water mixtures. Toluene was used for these experiments because it is relatively easy to determine its concentration in water by UV-Visible spectroscopy. The amount of toluene in water after filtering through the membranes is close to the informed solubility of toluene in water at 25 °C (0.53g/L, **[38]**) (**Figure 7**). The separation efficiency of these mixtures (η) was between 99.91% and 99.96 % (without any trend with **N**) defined as $\eta = 1 - \frac{X_{toluene}^{Filtered}}{X_{toluene}^{Initial}}$ where $X_{toluene}^{Initial}$ represents the molar fraction of toluene initially dispersed in water (above the membrane, before filtering) and $X_{toluene}^{Filtered}$ for the molar fraction of toluene dissolved in water, determined after filtering through the membrane.

Journal Pre-proofs

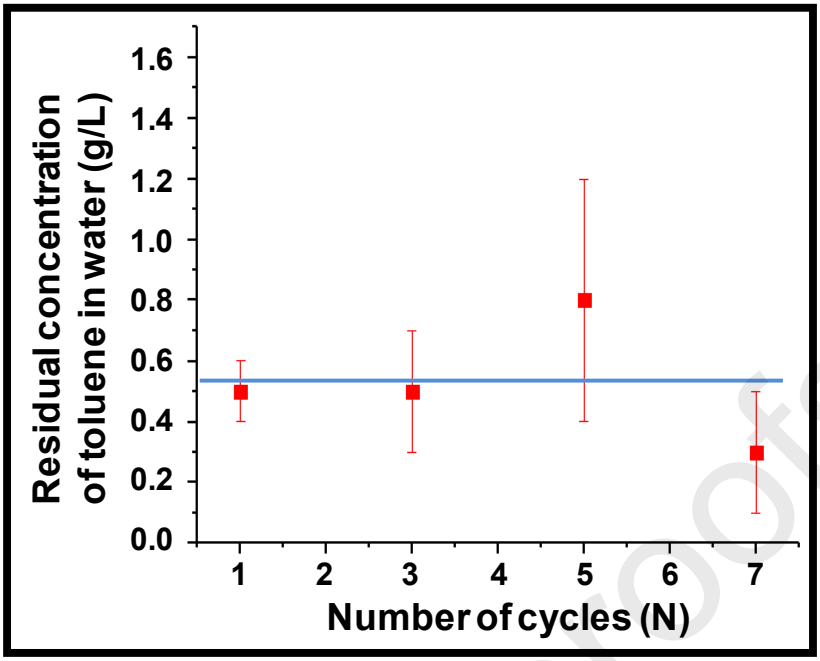

Figure 7. Residual concentration of toluene in water after filtering a water-toluene mixture through the setup of Figure 6. Horizontal line: solubility of toluene in water at 25 °C.

The calibration curves and UV absorption spectrum for spectroscopic determination of toluene in water are shown in **Supplementary Material** (**Figure S5**). There were no significant differences in the concentration of toluene in water with the number of immersion cycles during preparation, **N**. Several harsh conditions were investigated by exposing the membranes to saline water (NaCl 1M), hard water ($CaCl_2$, $MagCl_2$, 1M), acid solutions (HCl, pH= 3) and alkaline solutions (NaOH, pH= 11). In all cases, the membranes maintained their superwetting ability and the critical intrusion pressure ($\mathbf{P_c}$). In fact, no changes of the water-contact–angle (**WCA**) and $\mathbf{P_c}$ were observed when MQ-water, saline, hard-water, acid or alkaline solutions were used. The aspect and colour of the membranes are modified after immersing in acid solutions, but no changes in **WCA** and $\mathbf{P_c}$ were observed. The membranes maintained their quality parameters (flow rate, contact angles, separation efficiency and critical intrusion pressure) for at least three months (and possibly longer) when they are kept under permanent hydration conditions with distilled water.

Journal Pre-proofs

3.3 Flow characterization.

The water flux through the membranes presents a strong dependence with the number of immersion cycles, with values around 50 $Lm^{-2}s^{-1}$ for membranes with 3 cycles (**Figure 8**). It is observed a significant decrease of water flux with an increasing number of cycles, assigned to obstruction of pores by PAM, as shown in **Figure 8**.

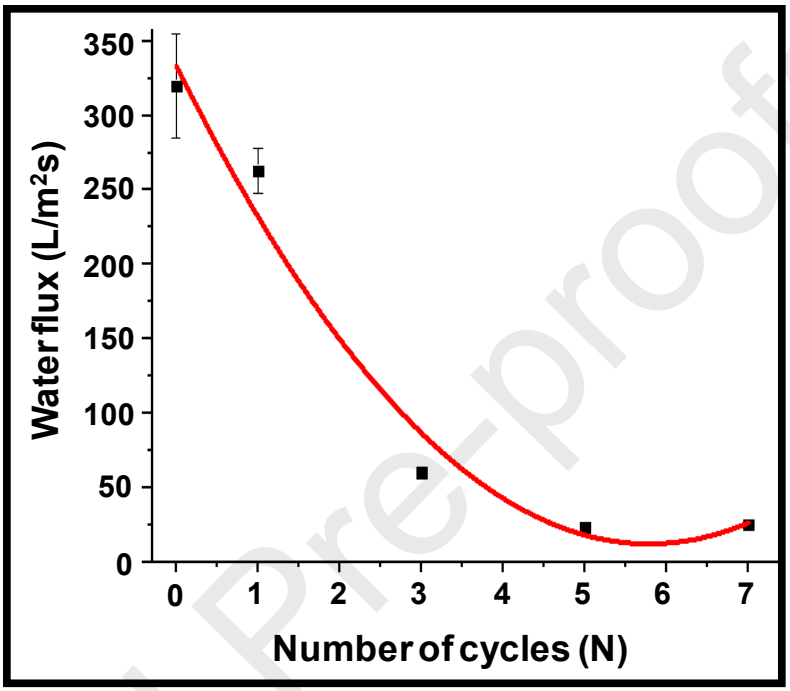

Figure 8. Water flux through PAM coated membranes. The height of the water column was fixed at 5 cm. Error bars are negligible in N=3, 5 and 7.

We propose a model for interpreting the results of **Figure 8**. Consider a metallic mesh whose filaments in absence of PAM (**N**=0) are separated by a distance L_0 (in the present study is L_0=77 μm). The area of the free pores in that case is L_0^2. After a given number **N** of immersion cycles in the polymerization media, the free pores area within L_0^2 is now $(L_0 - 2\varepsilon)^2$, where ε is the thickness of PAM coating around a metal filament. The area fraction of free pores in the area L_0^2 is $\phi_{porous} = \dfrac{(L_0 - 2\varepsilon)^2}{L_0^2}$ and the fraction of area occupied by PAM in the pores is:

$$\phi_{PAM} = 1 - \phi_{porous} = 4x(1-x) \qquad [i]$$

$$x \equiv \frac{\varepsilon}{L_0}, \quad 0 \le x \le \frac{1}{2} \qquad [ii]$$

We assume that water flows via two regions: i) through the open (non-coated) pores and ii) through regions of the original free-pores that are now coated with PAM. The contribution to the flow of coated regions just above the metal filament is neglected (for simplicity) in the model.

Thus, the total water flow, F (plotted in **Figure 8**), has two contributions in the developed model: $F = F_{pores} + F_{PAM}$. The model assumes that each flow is proportional to the respective fraction, ϕ_{porous} and ϕ_{PAM}: $F = k_1\phi_{pores} + k_2\phi_{PAM} = k_1 - (k_1 - k_2)\phi_{PAM}$. The constants k_1 and k_2 are given by the boundary conditions: $\phi_{PAM} = 0 \Rightarrow F = F_{MAX} = k_1$ and $\phi_{PAM} = 1 \Rightarrow F = F_{\min} = k_2$. Hence, $F = F_{MAX} - (F_{MAX} - F_{min})\phi_{PAM}$ is obtained. Using relationships [*i*] and [*ii*], a model expression for F in terms of x is obtained:

$$F = F_{MAX} - (F_{MAX} - F_{min})4x(1-x) \quad [iii]$$

The model parameter x is expected to increase with the amount of hydrogel coating. In the present work, the amount of PAM in the membranes is governed by the number of immersion cycles, **N**, used during preparation. The analysis of SEM images (like those of **Figure 1**) indicates that in fact x increases from **N**=0 to **N**=5, then reaching saturation between **N**=5 and 6. Below saturation, the relationship between x and **N** can be linearly approximated. We assume the simplest approach, that is, x proportional to **N** , which is a good empirical approximation to the experimental data (**Figure S6**, Supplementary Material) . The proportionality constant between x and **N** is given by the condition that at x=1/2 the pores are completely closed (filled with PAM), a condition reached after a given number of immersion cycles, referred as $\mathbf{N_{saturation}}$ in [*iv*]. Therefore:

$$x = \frac{1}{2}\frac{N}{N_{saturation}} \quad (0 \le x \le \frac{1}{2}) \quad [iv]$$

Expressions [*iii*] and [*iv*] were used to fit data of **Figure 8**. The recovered values are F_{MAX}=336 $Lm^{-2}s^{-1}$, F_{min}= 10 $Lm^{-2}s^{-1}$, $\mathbf{N_{saturation}}$ = 6. Note that the recovered values are in excellent agreement with the features observed in **Figure 8**: i) at **N**=0 is F=325 $Lm^{-2}s^{-1}$, close to the recovered F_{MAX}., ii) the flow reaches a minimum between 5 and 7 cycles (close to the recovered $\mathbf{N_{saturation}}$), iii) the minimum flow is about 25 $Lm^{-2}s^{-1}$ (close the recovered F_{min}).

Note that, as a remarkable difference with the contact angles, the flow F and the critical intrusion pressure $\mathbf{P_c}$ displays an important dependence with **N**. This behavior is connected to the two preparation stages. The first stage, APS pre-treatment, induces the required contact angles. The second stage, PAM coating, generates the condition for oil-water separation, related to F and $\mathbf{P_c}$.

The performance of the membranes is remarkable stable in time scales of several months. On the one hand, when drops of water are deposited on the air-membrane surface, these drops are immediately dispersed on the surface (and finally pass through), as illustrated in a Figure 3. On the other hand, in the oil/water separation experiments, the membranes are kept hydrated prior to their use, thus water forms a thin layer on both sides of the metal mesh. Both in the case of the deposited drop and in that of the hydrated membrane used in the separation tests, it was never observed that the pores of the membrane were sealed or clogged by the presence of water.

3.4 Bacteria adhesion

The effects on membrane performance due to the presence of bacteria is a complex issue, which naturally are expected to be more important for superhydrophilic than superhydrophobic membranes. A full study of those effects exceeds the objectives of the present work. Here, we present preliminary results about bacteria adhesion of a specific bacterium, *Pseudomona protegens***,** in order to illustrate the expected inconveniences in concrete applications at industrial level or when using natural waters. **Figure 9** illustrates the bacterial adhesion of *Pseudomonas protegens* on the membrane surfaces at different incubation times. As shown in **Figure 9**, the surface covered by bacteria increases with the immersion time of the membranes into a given bacterial growth media.

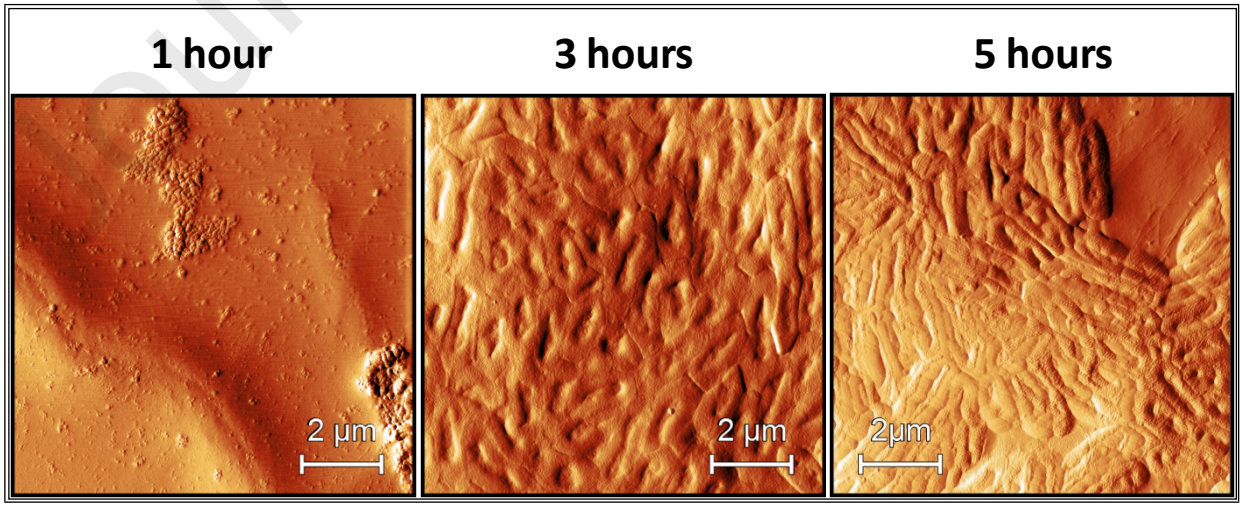

Figure 9. Samples immersed during different times (each) in a *Pseudomona protegens* culture. AFM images (amplitude error) of meshes sectors (on the metallic filaments). N= 5 in all cases.

As a first step, it appears reasonable to study the effect of the amount of PAM **(N)** on the bacteria adhesion over the membranes. When **N** increases, more PAM is coating the brass meshes, then bacteria are less exposed to copper and zinc, which as is well known they have bactericide effect. Therefore, this effect predicts increase of bacterial coverage with **N**. Besides, it is reported that topographical pattern surface have influence in the bacteria adhesion and biofilm development **[39]**, for instance the surface roughness **[40]**. The discrimination of the several possible morphological effects on biofilm formation is a challenging task. Here we just present experimental data of membrane roughness and bacterial coverage as function of **N**.

Figure 10 (top) shows representative AFM images of the membrane with different **N**. In **Figure 11** is shown (red square) membrane roughness, $\mathbf{R_a}$, as function of **N**. $\mathbf{R_a}$ was estimated using AFM height images registered on the metallic filament of the mesh, in the absence of bacteria which are shown in the Supplementary Material, **Figure S7**. As shown in **Figure 11**, membrane roughness decreases with increasing amounts (**N**) of hydrogel on the mesh. On the other hand, **Figure 11** (bottom) shows that biofilm formation is favoured by the presence of PAM, that is, the surface covered area by biofilm increases with **N** (fixing all other parameters). **Figure 11** (blue circle) illustrates these trends as a function of **N**.

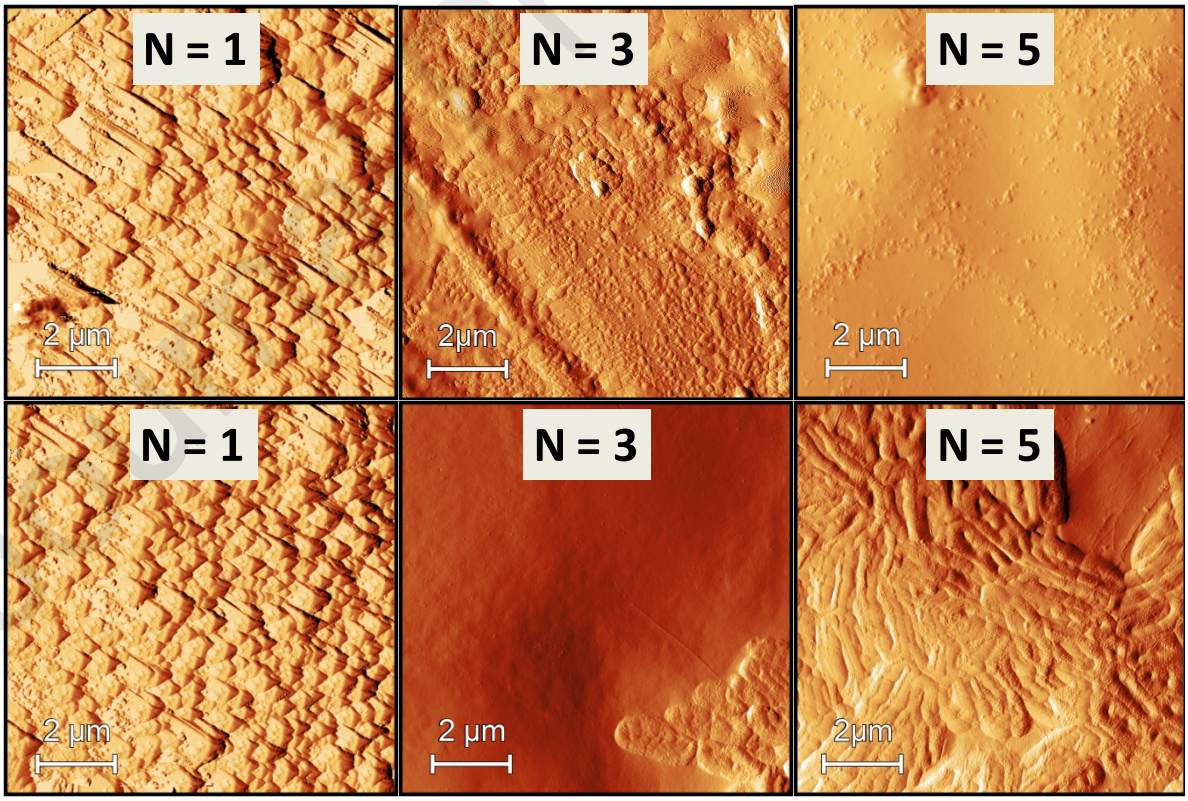

Figure 10. AFM images (amplitude error; 10 µm X 10 µm) of meshes sectors (on the metallic filaments) for different immersion cycles (N) without being in contact with bacteria cultures (top) and samples immersed 5 hours (each) in *Pseudomona protegens* cultures (OD=3) (bottom).

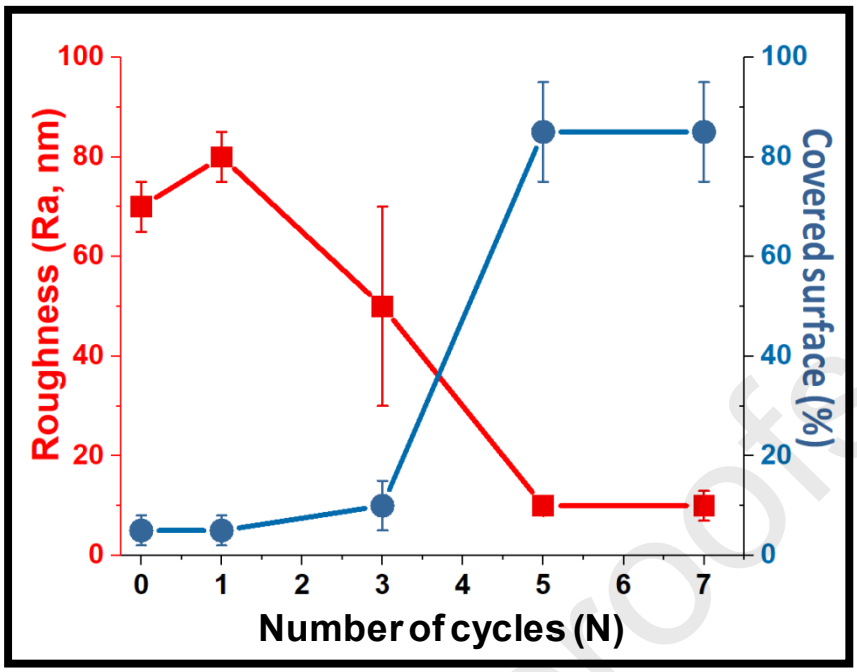

Figure 11. Red-Square points: roughness on the metallic filaments of membranes in the absence of bacteria. Blue-circled points: percentage of surface covered by *Pseudomona Protegens*, after immersing the membranes during 5 hours (each) in bacterial media.

As it was mentioned, the surface roughness parameter, $\mathbf{R_a}$, of membranes decreases with **N**, while the area of membranes covered by biofilms increases with **N**. A crossover of both trends is observed near **N** = 3. These preliminary results are of relevance for further membrane's performance, since showing that biofilm formation may seal the membranes, depending on bacterial concentration in the site.

4. Conclusions

The first remarkable result is that it was possible to obtain superhydrophilic PAM membranes without using UV-VIS irradiation for polymerization, which usually have low yields or require high intensity light sources. A two-steps redox process was used instead, that allows obtaining separation membranes with excellent properties in a simple and fast procedure. The method allows to systematically control the amount of hydrogel present in the membranes, a factor on which all properties of relevance for membranes used in oil-water separation are strongly dependent.

The use of APS was essential to achieve superhydrophilic membranes. Moreover, APS plays a central role in the two stages that constitute the total preparation process. The first stage was the so-called pre-treatment, which consists of oxidizing the mesh in an alkaline medium, controlling the conditions (concentration of APS and NaOH, temperature) in such a way that was possible to obtain copper oxides with homogenous nanometric morphology over the entire mesh. Therefore, nanostructures were obtained on the surface of the meshes, mostly nanobars but also nanopetals. The

presence of these structures was essential to ensure that the surface is uniformly wetted and to prevent highly inhomogeneous agglomeration of the compounds used in the subsequent polymerization step. Therefore, the first partial conclusion is that pre-treatment is necessary for obtaining superhydrophilic surfaces. This conclusion is coincident with that reported by Li *et al* for other meshes**[41]**.

Nevertheless, pre-treatment is not enough to obtain membranes. The second stage, polymer coating, is necessary to provide a non-null oil intrusion pressure. Meshes with the pre-treatment only, that is with the first stage exclusively, do not support oil column on it. The second stage consists of a redox polymerization to obtain PAM, where APS plays again a key role, now as redox initiator of polymerization. To the best of our knowledge, the only work reporting the redox polymerization of acrylamide for hydrocarbon-water separation systems is Chen *et al* **[42]**, who prepared nickel foams immersed in the mixture of precursors (APS, BIS, AM) to separate water-hydrocarbon, although the authors did not obtain separation membranes.

The described preparation method allowed us to study the effect of hydrogel amount formed on the substrate in a simple way by systematically changing the parameter **N**. The results indicate that water flow, critical inclusion pressure, surface roughness and the area covered by biofilms are strongly dependent on **N**. In particular, the mathematical model presented in this work allows predicting the flow of water through the membrane as a function of **N**, in the absence of bacteria.

The studies with bacteria suggest there is a value of **N** from which the coverage with bacteria has a strong influence on the quality parameters, with a percentage of sealed surface greater than 60% for **N**> 3 after 5 hours of immersing the membranes in a media with *Pseudomonas Protegens*. This result is of high practical as suggesting that biofilm formation is a critical factor for membranes with **N**≥3 (prepared under conditions used in this work). For example, the model developed confirms that high water flows are maintained for **N**≤3. On the other hand, the critical intrusion pressure is relatively low as **N** decreases below **N**=3. In the present studies, it seems that membranes with **N**≤3 are more appropriated to avoid the formation of biofilms, while maintaining significant water flows, at the cost of supporting low oil columns. However, the latter may not be an inconvenience in separation reactors with low differential pressure through the membranes. Therefore, for each specific application and situation, it is necessary to decide which the most relevant factor is.

Acknowledgments: NBD, LL and RMN are research members of the National Council of Research and Technology (CONICET, Argentina). JNC is owner of doctoral fellowship of CONICET. Financial support was received from UBA (UBACyT project 20020150100079BA,), Ministry of Science, Technology and Innovations (MINCYT- FONCYT, Argentina, PICT 2011-0377 and YPF Tecnología (YTEC). The authors thank Dr. Mario Contin (School of Pharmacy and Biochemistry, UBA) for the

DLS experiments and Dr. Andrea Amar (University of Córdoba, Argentina) for the RMN spectra with solid samples.

Conflicts of Interest: The authors declare no conflict of interest

References

(1) Jeevahan, J.; Chandrasekaran, M.; Britto Joseph, G.; Durairaj, R. B.; Mageshwaran, G. Superhydrophobic Surfaces: A Review on Fundamentals, Applications, and Challenges. *J Coat Technol Res* **2018**, *15* (2), 231–250. https://doi.org/10.1007/s11998-017-0011-x.

(2) Wang, Y.; Gong, X. Special Oleophobic and Hydrophilic Surfaces: Approaches, Mechanisms, and Applications. *J. Mater. Chem. A* **2017**, *5* (8), 3759–3773. https://doi.org/10.1039/C6TA10474F.

(3) Ma, W.; Samal, S. K.; Liu, Z.; Xiong, R.; De Smedt, S. C.; Bhushan, B.; Zhang, Q.; Huang, C. Dual PH- and Ammonia-Vapor-Responsive Electrospun Nanofibrous Membranes for Oil-Water Separations. *Journal of Membrane Science* **2017**, *537*, 128–139. https://doi.org/10.1016/j.memsci.2017.04.063.

(4) Zhang, M.; Ma, W.; Cui, J.; Wu, S.; Han, J.; Zou, Y.; Huang, C. Hydrothermal Synthesized UV-Resistance and Transparent Coating Composited Superoloephilic Electrospun Membrane for High Efficiency Oily Wastewater Treatment. *Journal of Hazardous Materials* **2020**, *383*, 121152. https://doi.org/10.1016/j.jhazmat.2019.121152.

(5) Ma, W.; Zhang, M.; Liu, Z.; Kang, M.; Huang, C.; Fu, G. Fabrication of Highly Durable and Robust Superhydrophobic-Superoleophilic Nanofibrous Membranes Based on a Fluorine-Free System for Efficient Oil/Water Separation. *Journal of Membrane Science* **2019**, *570–571*, 303–313. https://doi.org/10.1016/j.memsci.2018.10.035.

(6) Ma, W.; Zhang, M.; Liu, Z.; Huang, C.; Fu, G. Nature-Inspired Creation of a Robust Free-Standing Electrospun Nanofibrous Membrane for Efficient Oil–Water Separation. *Environ. Sci.: Nano* **2018**, *5* (12), 2909–2920. https://doi.org/10.1039/C8EN00895G.

(7) Sosa, M. D.; Lombardo, G.; Rojas, G.; Oneto, M. E.; Negri, R. M.; D'Accorso, N. B. Superhydrophobic Brass and Bronze Meshes Based on Electrochemical and Chemical Self-Assembly of Stearate. *Applied Surface Science* **2019**, *465*, 116–124. https://doi.org/10.1016/j.apsusc.2018.09.116.

(8) Ding, Y.; Wu, J.; Wang, J.; Lin, H.; Wang, J.; Liu, G.; Pei, X.; Liu, F.; Tang, C. Y. Superhydrophilic and Mechanical Robust PVDF Nanofibrous Membrane through Facile Interfacial Span 80 Welding for Excellent Oil/Water Separation. *Applied Surface Science* **2019**, *485*, 179–187. https://doi.org/10.1016/j.apsusc.2019.04.214.

(9) Zhao, P.; Qin, N.; Ren, C. L.; Wen, J. Z. Polyamide 6.6 Separates Oil/Water Due to Its Dual Underwater Oleophobicity/Underoil Hydrophobicity: Role of 2D and 3D Porous Structures. *Applied Surface Science* **2019**, *466*, 282–288. https://doi.org/10.1016/j.apsusc.2018.10.041.

(10) Liu, Z.; Qin, D.; Zhao, J.; Feng, Q.; Li, Z.; Bai, H.; Sun, D. D. Efficient Oil/Water Separation Membrane Derived from Super-Flexible and Superhydrophilic Core–Shell Organic/Inorganic Nanofibrous Architectures. *Polymers* **2019**, *11* (6), 974. https://doi.org/10.3390/polym11060974.

(11) Wang, X.; Zeng, J.; Yu, X.; Liang, C.; Zhang, Y. Water Harvesting Method via a Hybrid Superwettable Coating with Superhydrophobic and Superhydrophilic Nanoparticles. *Applied Surface Science* **2019**, *465*, 986–994. https://doi.org/10.1016/j.apsusc.2018.09.210.

(12) Gondal, M. A.; Sadullah, M. S.; Qahtan, T. F.; Dastageer, M. A.; Baig, U.; McKinley, G. H. Fabrication and Wettability Study of WO3 Coated Photocatalytic Membrane for Oil-Water Separation: A Comparative Study with ZnO Coated Membrane. *Sci Rep* **2017**, *7* (1), 1686. https://doi.org/10.1038/s41598-017-01959-y.

(13) Zhang, D.; Wang, G.; Zhi, S.; Xu, K.; Zhu, L.; Li, W.; Zeng, Z.; Xue, Q. Superhydrophilicity and Underwater Superoleophobicity TiO2/Al2O3 Composite Membrane with Ultra Low Oil Adhesion for Highly Efficient Oil-in-Water Emulsions Separation. *Applied Surface Science* **2018**, *458*, 157–165. https://doi.org/10.1016/j.apsusc.2018.07.052.

(14) Yu, J.; Zeng, W.; Fu, X.; Zheng, Y.; Huang, J.; Sun, D. High-Flux and Robust Co_3O_4 Mesh for Efficient Oil/Water Separation in Harsh Environment. *ACS Omega* **2019**, *4* (4), 7385–7390. https://doi.org/10.1021/acsomega.9b00415.

(15) Xie, A.; Dai, J.; Ma, C.; Cui, J.; Chen, Y.; Lang, J.; Gao, M.; Li, C.; Yan, Y. Construction of Caterpillar-like Cobalt-Nickel Hydroxide/Carbon Cloth Hierarchical Architecture with Reversible Wettability towards on-Demand Oil-Water Separation. *Applied Surface Science* **2018**, *462*, 659–668. https://doi.org/10.1016/j.apsusc.2018.08.161.

(16) Ge, B.; Han, L.; Liang, X.; Li, F.; Pu, X.; Zhu, X.; Zhang, Z.; Shao, X.; Jin, C.; Li, W. Fabrication of Superhydrophobic Cu-BiOBr Surface for Oil/Water Separation and Water Soluble Pollutants Degradation. *Applied Surface Science* **2018**, *462*, 583–589. https://doi.org/10.1016/j.apsusc.2018.08.174.

(17) Zhang, P.; Zhao, C.; Zhao, T.; Liu, M.; Jiang, L. Recent Advances in Bioinspired Gel Surfaces with Superwettability and Special Adhesion. *Adv. Sci.* **2019**, *6* (18), 1900996. https://doi.org/10.1002/advs.201900996.

(18) Raviv, U. Fluidity of Bound Hydration Layers. *Science* **2002**, *297* (5586), 1540–1543. https://doi.org/10.1126/science.1074481.

(19) Xue, Z.; Wang, S.; Lin, L.; Chen, L.; Liu, M.; Feng, L.; Jiang, L. A Novel Superhydrophilic and Underwater Superoleophobic Hydrogel-Coated Mesh for Oil/Water Separation. *Adv. Mater.* **2011**, *23* (37), 4270–4273. https://doi.org/10.1002/adma.201102616.

(20) Sun, M.; Zhao, S.; Wei, W.; Wu, J.; Wang, J. Polyacrylamide-Modified Polyester Fabric with Easy-Cleaning for Efficient Oil/Water Separation. *aatcc j res* **2018**, *5* (1), 1–6. https://doi.org/10.14504/ajr.5.1.1.

(21) Liu, M.; Wang, S.; Wei, Z.; Song, Y.; Jiang, L. Bioinspired Design of a Superoleophobic and Low Adhesive Water/Solid Interface. *Adv. Mater.* **2009**, *21* (6), 665–669. https://doi.org/10.1002/adma.200801782.

(22) Madhuranthakam, C. M. R.; Alsubaei, A.; Elkamel, A. Performance of Polyacrylamide and Poly(Acrylamide/Sodium Acrylate) Hydrogel-Coated Mesh for Separation of Oil/Water Mixtures. *Journal of Water Process Engineering* **2018**, *26*, 62–71. https://doi.org/10.1016/j.jwpe.2018.09.009.

(23) Liu, Y.; Su, Y.; Cao, J.; Guan, J.; Zhang, R.; He, M.; Fan, L.; Zhang, Q.; Jiang, Z. Antifouling, High-Flux Oil/Water Separation Carbon Nanotube Membranes by Polymer-Mediated Surface

Charging and Hydrophilization. *Journal of Membrane Science* **2017**, *542*, 254–263. https://doi.org/10.1016/j.memsci.2017.08.018.

(24) Ang, M. B. M. Y.; Ji, Y.-L.; Huang, S.-H.; Tsai, H.-A.; Hung, W.-S.; Hu, C.-C.; Lee, K.-R.; Lai, J.-Y. Incorporation of Carboxylic Monoamines into Thin-Film Composite Polyamide Membranes to Enhance Nanofiltration Performance. *Journal of Membrane Science* **2017**, *539*, 52–64. https://doi.org/10.1016/j.memsci.2017.05.062.

(25) Wang, J.-C.; Lou, H.; Cui, Z.-H.; Hou, Y.; Li, Y.; Zhang, Y.; Jiang, K.; Shi, W.; Qu, L. Fabrication of Porous Polyacrylamide/Polystyrene Fibrous Membranes for Efficient Oil-Water Separation. *Separation and Purification Technology* **2019**, *222*, 278–283. https://doi.org/10.1016/j.seppur.2019.04.044.

(26) Yao, M.; Nan, J.; Chen, T.; Zhan, D.; Li, Q.; Wang, Z.; Li, H. Influence of Flocs Breakage Process on Membrane Fouling in Coagulation/Ultrafiltration Process—Effect of Additional Coagulant of Poly-Aluminum Chloride and Polyacrylamide. *Journal of Membrane Science* **2015**, *491*, 63–72. https://doi.org/10.1016/j.memsci.2015.05.018.

(27) Yu, W.; Liu, H.; Xu, L.; Qu, J.; Graham, N. The Pre-Treatment of Submerged Ultrafiltration Membrane by Coagulation—Effect of Polyacrylamide as a Coagulant Aid. *Journal of Membrane Science* **2013**, *446*, 50–58. https://doi.org/10.1016/j.memsci.2013.06.012.

(28) Yang, D.; Sun, Y.; Ghadiri, M.; Wu, H.; Qiao, H.; He, L.; Luo, X.; Lü, Y. Effect of Hydrolyzed Polyacrylamide Used in Polymer Flooding on Droplet–Interface Electro-Coalescence: Variation of Critical Electric Field Strength of Partial Coalescence. *Separation and Purification Technology* **2019**, *227*, 115737. https://doi.org/10.1016/j.seppur.2019.115737.

(29) Ma, J.; Shi, J.; Ding, L.; Zhang, H.; Zhou, S.; Wang, Q.; Fu, X.; Jiang, L.; Fu, K. Removal of Emulsified Oil from Water Using Hydrophobic Modified Cationic Polyacrylamide Flocculants Synthesized from Low-Pressure UV Initiation. *Separation and Purification Technology* **2018**, *197*, 407–417. https://doi.org/10.1016/j.seppur.2018.01.036.

(30) Videla, H. A.; Herrera, L. K. Microbiologically Influenced Corrosion: Looking to the Future. *Int. Microbiol.* **2005**, *8* (3), 169–180.

(31) Zhang, W.; Wen, X.; Yang, S.; Berta, Y.; Wang, Z. L. Single-Crystalline Scroll-Type Nanotube Arrays of Copper Hydroxide Synthesized at Room Temperature. *Adv. Mater.* **2003**, *15* (10), 822–825. https://doi.org/10.1002/adma.200304840.

(32) Cabrera, J.; Ruiz, M.; Fascio, M.; D'Accorso, N.; Mincheva, R.; Dubois, P.; Lizarraga, L.; Negri, R. Increased Surface Roughness in Polydimethylsiloxane Films by Physical and Chemical Methods. *Polymers* **2017**, *9* (12), 331. https://doi.org/10.3390/polym9080331.

(33) Lević, S.; Pajić Lijaković, I.; Đorđević, V.; Rac, V.; Rakić, V.; Šolević Knudsen, T.; Pavlović, V.; Bugarski, B.; Nedović, V. Characterization of Sodium Alginate/d-Limonene Emulsions and Respective Calcium Alginate/d-Limonene Beads Produced by Electrostatic Extrusion. *Food Hydrocolloids* **2015**, *45*, 111–123. https://doi.org/10.1016/j.foodhyd.2014.10.001.

(34) Díaz, C.; Salvarezza, R. C.; Fernández Lorenzo de Mele, M. A.; Schilardi, P. L. Organization of *Pseudomonas Fluorescens* on Chemically Different Nano/Microstructured Surfaces. *ACS Appl. Mater. Interfaces* **2010**, *2* (9), 2530–2539. https://doi.org/10.1021/am100313z.

(35) Díaz, C.; Schilardi, P. L.; Salvarezza, R. C.; Fernández Lorenzo de Mele, M. Nano/Microscale Order Affects the Early Stages of Biofilm Formation on Metal Surfaces. *Langmuir* **2007**, *23* (22), 11206–11210. https://doi.org/10.1021/la700650q.

(36) Kelleher, S. M.; Habimana, O.; Lawler, J.; O' Reilly, B.; Daniels, S.; Casey, E.; Cowley, A. Cicada Wing Surface Topography: An Investigation into the Bactericidal Properties of Nanostructural Features. *ACS Appl. Mater. Interfaces* **2016**, *8* (24), 14966–14974. https://doi.org/10.1021/acsami.5b08309.

(37) Xu, L.; Che, L.; Zheng, J.; Huang, G.; Wu, X.; Chen, P.; Zhang, L.; Hu, Q. Synthesis and Thermal Degradation Property Study of N-Vinylpyrrolidone and Acrylamide Copolymer. *RSC Adv.* **2014**, *4* (63), 33269–33278. https://doi.org/10.1039/C4RA05720A.

(38) Sanemasa, I.; Araki, M.; Deguchi, T.; Nagai, H. Solubility Measurements of Benzene and the Alkylbenzenes in Water by Making Use of Solute Vapor. *BCSJ* **1982**, *55* (4), 1054–1062. https://doi.org/10.1246/bcsj.55.1054.

(39) Anselme, K.; Davidson, P.; Popa, A. M.; Giazzon, M.; Liley, M.; Ploux, L. The Interaction of Cells and Bacteria with Surfaces Structured at the Nanometre Scale. *Acta Biomaterialia* **2010**, *6* (10), 3824–3846. https://doi.org/10.1016/j.actbio.2010.04.001.

(40) Tripathy, A.; Sen, P.; Su, B.; Briscoe, W. H. Natural and Bioinspired Nanostructured Bactericidal Surfaces. *Advances in Colloid and Interface Science* **2017**, *248*, 85–104. https://doi.org/10.1016/j.cis.2017.07.030.

(41) Li, X.; Zhang, W.; Liu, N.; Qu, R.; Wei, Y.; Feng, L. Superwetting Copper Meshes Based on Self-Organized Robust CuO Nanorods: Efficient Water Purification for *in Situ* Oil Removal and Visible Light Photodegradation. *Nanoscale* **2018**, *10* (9), 4561–4569. https://doi.org/10.1039/C7NR09201F.

(42) Chen, B.; Ju, G.; Sakai, E.; Qiu, J. Underwater Low Adhesive Hydrogel-Coated Functionally Integrated Device by a One-Step Solution-Immersion Method for Oil–Water Separation. *RSC Adv.* **2015**, *5* (106), 87055–87060. https://doi.org/10.1039/C5RA13657A.

(43) Magalhães, A. S. G.; Almeida Neto, M. P.; Bezerra, M. N.; Ricardo, N. M. P. S.; Feitosa, J. P. A. Application of Ftir in the Determination of Acrylate Content in Poly(Sodium Acrylate-Co-Acrylamide) Superabsorbent Hydrogels. *Quím. Nova* **2012**, *35* (7), 1464–1467. https://doi.org/10.1590/S0100-40422012000700030.

(44) Jonathan, N. The Infrared and Raman Spectra and Structure of Acrylamide. *Journal of Molecular Spectroscopy* **1961**, *6*, 205–214. https://doi.org/10.1016/0022-2852(61)90243-0.

(45) Al-Sabagh, A. M.; Kandile, N. G.; El-Ghazawy, R. A.; Noor El-Din, M. R.; El-sharaky, E. A. Synthesis and Characterization of High Molecular Weight Hydrophobically Modified Polyacrylamide Nanolatexes Using Novel Nonionic Polymerizable Surfactants. *Egyptian Journal of Petroleum* **2013**, *22* (4), 531–538. https://doi.org/10.1016/j.ejpe.2013.11.007.

Journal Pre-proofs

SUPPLEMENTARY MATERIAL

Membranes Based on Polyacrylamide Coatings on Metallic Meshes Prepared by a Two-Steps Redox Polymerization.

J. Nicolás Cabrera, Graciela Rojas, Norma B. D´Accorso, Leonardo Lizarraga, R. Martín Negri

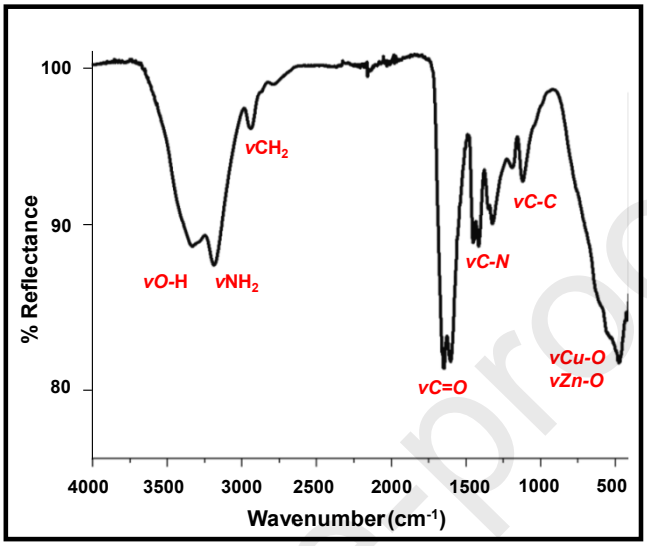

Figure S1. FTIR (ATR) spectra of PAM coated membrane. Functional groups associated to bands are indicated.

In **Figure S1**, peaks around 400–900 cm^{-1} are assigned to metal–oxygen stretching of CuO and ZnO (resulted from the oxidation of the membrane with APS). The bands around 3400 cm^{-1} (NH_2), 2900 cm^{-1} (CH_2) and 1700 cm^{-1} (C=O) are the expected bands of PAM **[43, 44]**.

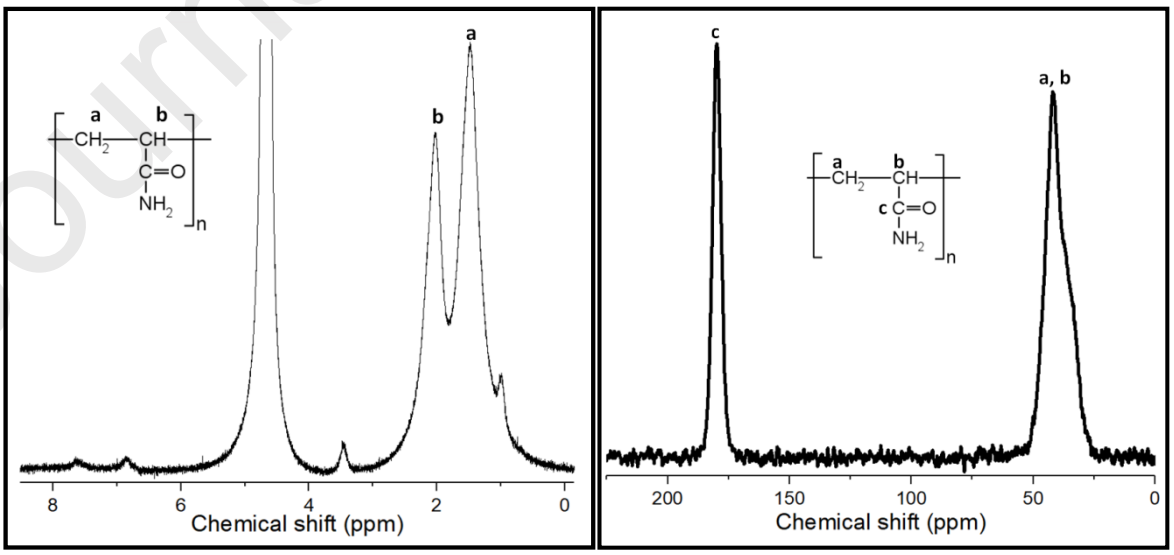

Figure S2: NMR of PAM. A) ^{1}H NMR spectrum in D_2O as solvent and TMS as internal standard, performed in a Bruker 200 MHz; B) ^{13}C NMR spectrum of a solid sample was performed in 7T Bruker Avance II-300 spectrometer 75.46mHz.

In the ^{1}H NMR spectrum of PAM performed in gel state, it is possible to observe the methine and methylene signals at 1.5 ppm and 2 ppm respectively. The signals at 4.8 ppm corresponding to protons of water residues, meanwhile the little signals around 3.5 ppm can be attributed to vinylic protons associated with partially unreacted crosslinker (See **Figure S2A**). 13C NMR spectrum of PAM in solid phase is shown in **Figure S2B**, where methine and methylene signals appear together between 25 and 50ppm and the carbonyl signal appears around 180ppm. These results are consistent with previously reported data **[45]**.

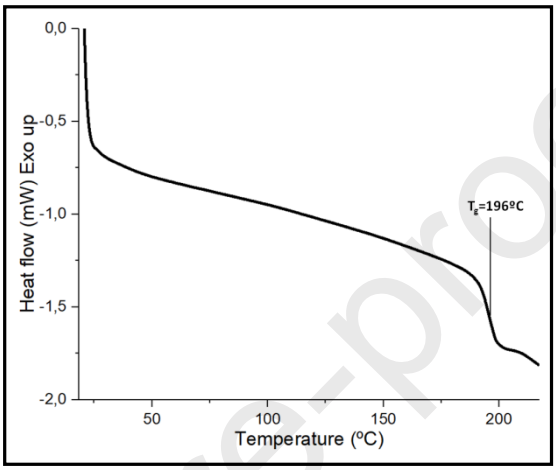

Figure S3: DSC results of synthesized polyacrylamide.

The glass transition temperature (T_g) obtained from **Figure S3** is consistent with reported values for polyacrylamide **[37]**.

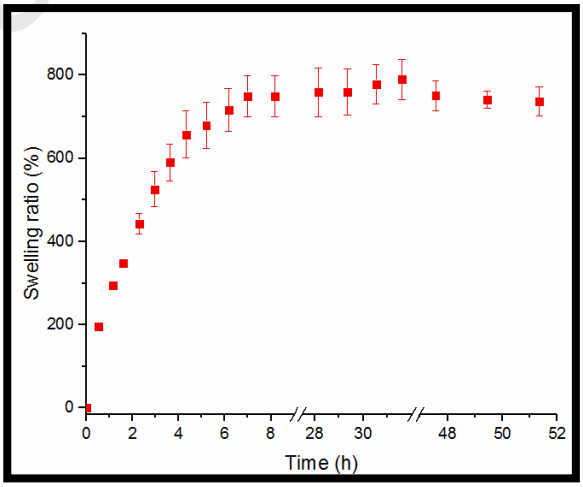

Figure S4: water-polymer swelling test. A sample of PAM is immersed in distilled water at t=0. Then is weighted at different time, the mass increases is recorded, and the sample is placed back into the solution. The percentage of mass increase (swelling ratio) is plotted as function of time.

1.

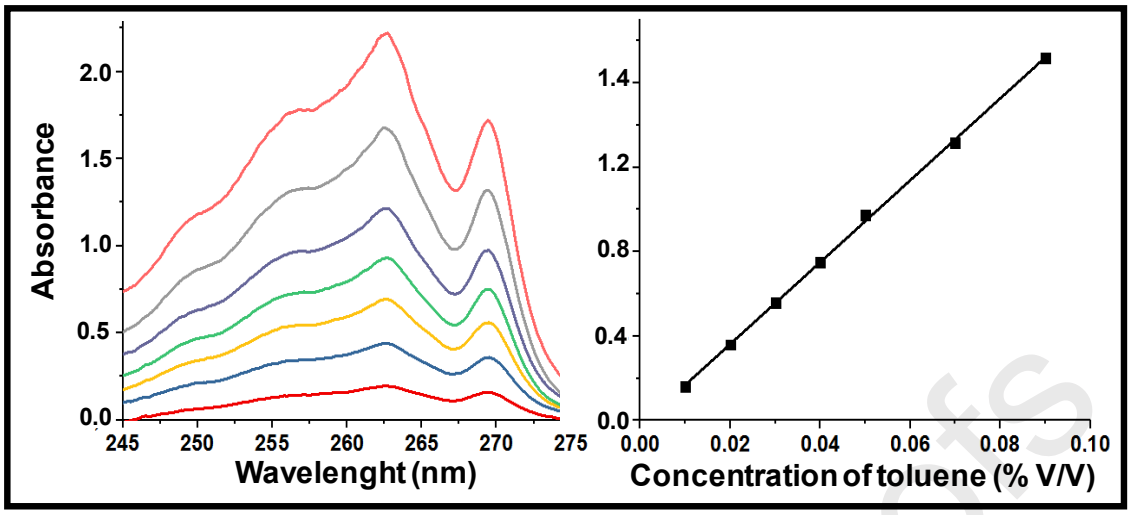

2. **Figure S5.** **Absorbance spectrum of toluene in chloroform at different concentration (left) and calibration curve of toluene in chloroform at 270 nm (right).**

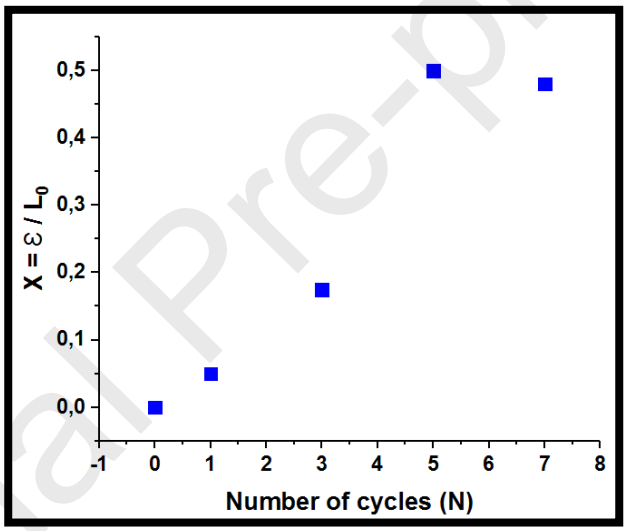

Figure S6. Dependence of *x* with N from SEM images. N is the number of immersion cycles. The parameter *x* is defined as the thickness of PAM coating around a metal filament, ε, divided by the length between filaments, L_0.

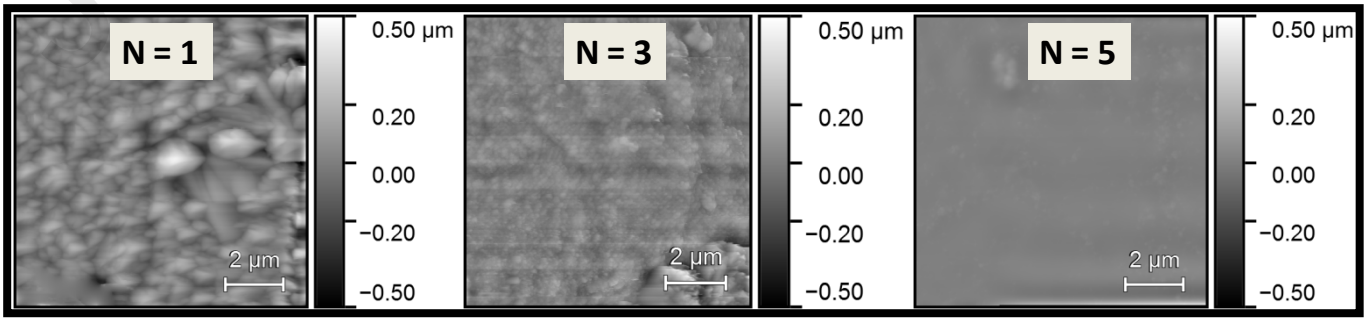

Figure S7. AFM Height images used for average surface roughness (R_a) determination.

Highlights

- PAM superhydrophilic membranes were prepared by a two-step oxidative polymerization.
- The performance parameters of oil-water separation were studied.
- A model for water flow as function of hydrogel coverage was developed.
- Bacterial adhesion of *Pseudomona protegens* was investigated as function of PAM coverage.

Journal Pre-proofs

Author statement:

J.N.Cabrera performed and analyzed all experiments.

G.Rojas: mesh characterization and discussion.

N.B. D´ Acorsso: polymer characterization.

L.Lizarraga: bacterial adhesión.

R.M.Negri: oil-water separation.

Journal Pre-proofs

Declaration of interests

X The authors declare that they have no known competing financial interests or personal relationships that could have appeared to influence the work reported in this paper.

☐The authors declare the following financial interests/personal relationships which may be considered as potential competing interests:

None

Journal Pre-proofs